

# Direct evidence of angle-selective transmission of Dirac electrons in graphene p-n junctions

Atikur Rahman, Janice Wynn Guikema, and Nina Marković

*Department of Physics and Astronomy, Johns Hopkins University, Baltimore, Maryland 21218, USA.*

The relativistic nature of the charge carriers in graphene is manifested in the angle-dependent transmission across p-n junctions, where Klein tunneling involves annihilation of an electron and a hole at the p-n junction interface. The transmission probability is equal to unity and independent of the barrier height for normal incidence, and it oscillates as a function of barrier height for other incident angles. Here we demonstrate the angle dependence of the resistance fluctuations of ballistic dual-gated graphene devices with straight and angled arms, in which the barrier height is controlled by a shared gate electrode. We find large fluctuations in the resistance as a function of gate voltage in the case of Klein tunneling at a  $45^\circ$  angle, as compared to normal incidence. Using a balancing measurement technique, we isolate the angle dependence of the resistance fluctuations from other angle insensitive gate-dependent and device-dependent effects. Our results provide a direct evidence of the angle-selective transmission of charge carriers in graphene p-n junctions, which is the key element behind focusing of electrons and the realization of a Veselago lens in graphene.

Charge carriers in graphene behave like massless, relativistic particles [1–4], characterized by chirality which arises from the existence of two interpenetrating sublattices in the hexagonal crystal structure of graphene. Due to the chiral nature of the charge carriers, back scattering by impurities is forbidden [5, 6], giving rise to unusual effects in graphene p-n junctions such as Klein tunneling, electron lensing and collimation [7–17]. As a result of the charge conjugation-like symmetry between electrons and holes, Klein tunneling in graphene involves an annihilation of an electron and a hole at the p-n junction interface [10]. For a ballistic p-n junction, the transmission probability is equal to unity for normally incident charge carriers (incident angle  $\phi = 0^\circ$ , with respect to the junction normal). Away from the normal incidence ( $\phi \neq 0$ ), the transmission probability oscillates as a function of the incident angle for a fixed barrier height [10]. For a fixed incident angle, other than normal incidence, the transmission probability also oscillates with varying barrier height.

Signatures of Klein tunneling in graphene have been found in the asymmetry in the resistance with respect to the gate voltage [18, 19], conductance oscillations [20, 21], resistance measurements [22], and electron guiding [23]. Asymmetry in the resistance-gate voltage characteristics has been attributed to the difference between the Klein tunneling and over-barrier transmission [24]. Resistance of a p-n junction also depends on the smoothness of the junction in the ballistic limit and on the screening effects [25, 26]. In the ballistic regime, conductance oscillations as a function of gate voltage have been interpreted as interference between forward and backward scattered wavefunctions between the two p-n interfaces [11]. However, the experiments are typically done in the two-terminal geometry [18–23, 27], in which case the contact effects are unavoidable [21, 28–31] and can be difficult to take into account.

Here we report a direct measurement of angle-

dependent resistance fluctuations as a function of barrier height that arise due to Klein tunneling of charge carriers across p-n junctions in graphene. Using ballistic pn junction devices with straight and angled arms (shown in Fig. 1(a)) and a balancing measurement technique, we separate out the angle-dependent effects from other gate-dependent angle insensitive resistances.

Graphene flakes were mechanically exfoliated from natural flake graphite and deposited on a Si wafer coated with 300 nm  $\text{SiO}_2$  [1, 2]. Single-layer flakes were identified by optical microscope and confirmed by Raman spectroscopy. Electrical leads were patterned by standard optical and e-beam lithography and the contacts were thermally evaporated (5nm Cr/ 75nm Au). Oxygen plasma (100 W for 45 sec) was used to pattern the graphene. To fabricate the top gate, 20 nm of  $\text{Al}_2\text{O}_3$  was deposited as the top gate insulating layer, followed by deposition of a 200 nm wide gold electrode on top. Scanning electron microscope (SEM) image of a typical device is shown in Fig. 1(a).

Electrical measurements were carried out at 4.2 K by placing the samples in vacuum in a He3 cryostat. The bias current was kept sufficiently low to avoid heating. Measurements were done in a four probe geometry with external voltage probes [31], using the SR 560 low noise preamplifier and PAR 124A analog lock-in amplifier equipped with an EG&G 116 preamplifier (operating in differential mode).

The resistance as a function of the back gate voltage ( $V_{Bg}$ ) and the top gate voltage ( $V_{Tg}$ ) is shown in Fig. 1(b) and 1(c) for a typical device, measured on the straight arm at 4.2 K. The shift of the Dirac point or the charge neutrality point (CNP) is evident from the data. With a suitable combination of  $V_{Bg}$  and  $V_{Tg}$ , all portions of the graphene device can be p or n type, or one can make a p-n\*-p or an n-p\*-n structure (where n\* and p\* denote the carrier type under the top gate).

In order to isolate the angle-dependent transmission of

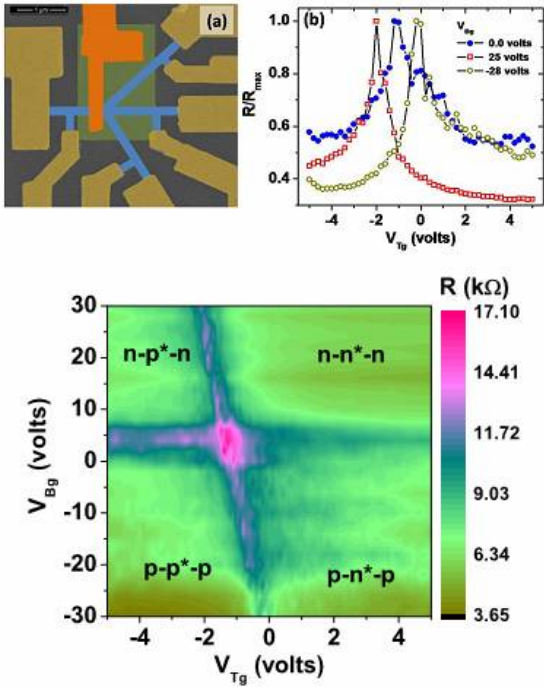


FIG. 1: (a) False color SEM micrograph of a patterned single layer graphene device with straight and angled arms (blue). The straight arms are perpendicular to the top gate, and the angled arms form a  $45^\circ$  angle with the top gate. The top gate (shown in orange) is placed at the point where the straight and angled arms meet. The gate dielectric is shown in green (20 nm of  $\text{Al}_2\text{O}_3$ ), and the leads are yellow (5nm Cr/ 75nm Au). The scale bar is  $1 \mu\text{m}$  long. (b) Normalized resistance as a function of the top gate voltage for three different values of back gate voltage measured on the straight arm (device SL1). (c) Color plot of the resistance as a function of back gate and top gate voltage measured on the straight arm (device SL2). The shift of the charge neutrality point as a function of  $V_{Bg}$  and  $V_{Tg}$  is evident, clearly defining regimes in which the device forms an  $n\text{-p}^*\text{-n}$ ,  $n\text{-n}^*\text{-n}$ ,  $p\text{-p}^*\text{-p}$  or a  $p\text{-n}^*\text{-p}$  structure ( $n^*$  and  $p^*$  denote the carrier type under the top gate)

charge carriers across a p-n junction, we used a balancing measurement technique, as shown in Fig. 2(a). The graphene device has three arms (1-2, 1-3 and 1-4) which share a common top-gated portion, placed just before the branching point. The resistance as a function of  $V_{Tg}$  for  $V_{Bg} = 30$  volts is shown in Fig. 2(b) for all three arms.

In the measurements described below, we use two arms at the time, either one straight and one angled, or two angled arms (measurements on 1-2 and 1-3 are shown on the schematic in Fig. 2(a), but we have also measured 1-2 and 1-4, and 1-3 and 1-4). The current branching between the two arms of the device is balanced (with the help of variable resistor) in such a way that, in the absence of top gate voltage, the voltage difference between the two arms (2 and 3 shown in Fig. 2(a)), measured

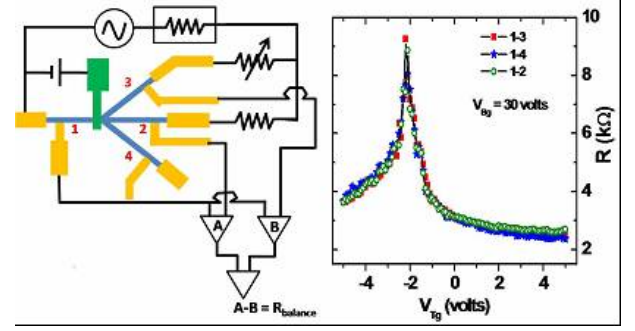


FIG. 2: (a) Measurement schematic used to study the angle-dependent resistance through the deviation from the balanced condition as a function of  $V_{Tg}$ . In this schematic, the current branching in the arms 1-2 and 1-3 are balanced (using a variable resistor) in such a way that the voltage difference between A and B is zero when  $V_{Tg}=0$  (arm 1-4 is not connected on this schematic). The deviation in resistance from the balanced condition, ( $R_{balance}$ ), is then measured as a function of  $V_{Tg}$ . (b) Resistance as a function of top gate voltage for device SL1. Nearly the same effect of  $V_{Tg}$  on all three arms reflects the fact that all three arms share the same gated portion.

with respect to ground, is minimum (limited by the background noise of few nanovolts). Any change in the ratio of the current flow in the two arms will be measured as a deviation from this balanced condition. Since the two arms share the top-gated portion, they will also share any angle insensitive gate-dependent effects, which will not cause a deviation from the balanced condition. A deviation from the balanced condition as a function of the voltage on the top gate can therefore separate the angle-dependent resistance from the effects of gate-dependent angle insensitive resistances [27].

For a particular back gate voltage, we first balance two of the arms (say 1-2 and 1-3) at zero top gate voltage. Then, we study the deviation of the resistance from the balanced condition as a function of top gate voltage. The change in the resistance from the balanced condition ( $R_{balance}$ ) as a function of  $V_{Tg}$  is shown in Fig. 3(a) (the balancing was done at  $V_{Bg} = -28$  volts and  $V_{Tg} = 0$ ). It is apparent that the amplitude of the fluctuations in ( $R_{balance}$ ) is smaller for negative values of  $V_{Tg}$ . Similarly, if we balance the bridge at  $V_{Bg} = 25$  volts and  $V_{Tg} = 0$ , larger fluctuations in ( $R_{balance}$ ) are observed below  $V_{Tg} = -2$  volts (see Fig. 3(b)). The derivative of  $R_{balance}$  as a function of  $V_{Tg}$  ( $dR_{balance}/dV_{Tg}$ ) is shown in Fig. 3(c) as a function of  $V_{Tg}$ , along with the corresponding change in resistance. It is clear that the fluctuations are significantly larger in the  $p\text{-n}^*\text{-p}$  side than in the  $p\text{-p}^*\text{-p}$  side. Similarly, larger fluctuations are observed in the  $n\text{-p}^*\text{-n}$  side compared to the  $n\text{-n}^*\text{-n}$  side of the top gate voltage (Fig. 3(d)).

To get a more quantitative measure of the fluctuations, we divided the data points into small bins and calculated the standard deviation of  $dR_{balance}/V_{Tg}$  as a function of

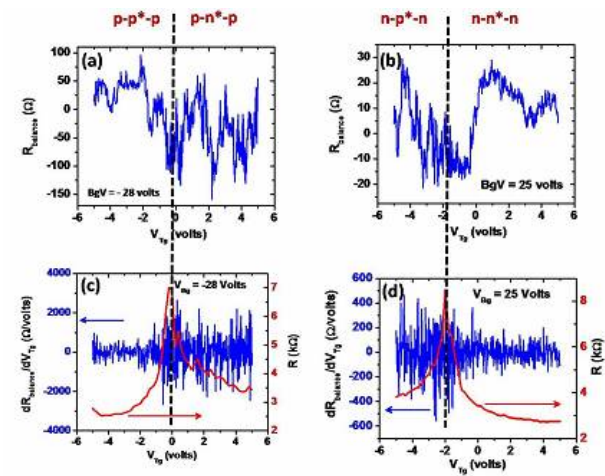


FIG. 3:  $R_{balance}$  as a function of  $V_{Tg}$  for (a)  $V_{Bg}=-28$  volts and (b)  $V_{Bg}=25$  volts.  $R_{balance}$  is measured by balancing arms 1-2 and 1-3, as shown in the schematic in Fig. 2(a). Corresponding derivatives of  $R_{balance}$  with respect to  $V_{Tg}$  is shown in (c) for  $V_{Bg}=-28$  volts and (d) for  $V_{Bg}=25$  volts (left axis). The corresponding change in resistance is shown in red (right axis). It is evident that the amplitude of the fluctuations in  $R_{balance}$  is larger in the p-n\*-p and n-p\*-n regimes than in the p-p\*-p and n-n\*-n regimes.

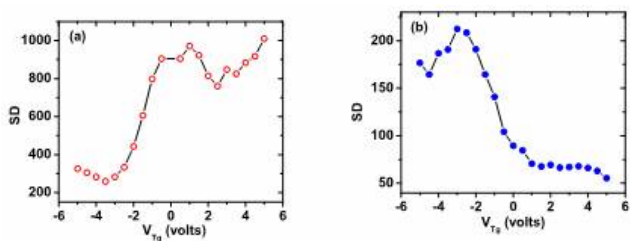


FIG. 4: (a) Standard deviation of  $dR_{balance}/dV_{Tg}$  as a function of  $V_{Tg}$  for (a)  $V_{Bg} = -28$  volts and (b)  $V_{Bg} = 25$  volts. The standard deviation of  $dR_{balance}/dV_{Tg}$  increases up to four times as the variation of  $V_{Tg}$  takes the device from the p-p\*-p to p-n\*-p or from n-n\*-n to n-p\*-n regime.

$V_{Tg}$ . Fig. 4(a) and (b) show the standard deviation (SD) calculated with twenty five data points per bin and averaged over four data points. It is evident that the standard deviation of the fluctuations increases significantly as we cross from p-p\*-p to p-n\*-p or from n-n\*-n to n-p\*-n region. It is interesting to note that the standard deviation of the fluctuations is larger on the p-n\*-p side than on the n-p\*-n side.

The mean free path ( $l_{mfp}$ ) is estimated to be around  $\sim 220$  nm, and the width of the top gate is 200 nm. This means that the electrons can travel ballistically through each pn junction and the entire region under the top gate. Ballistic transport across a graphene p-n junction is expected to result in perfect transmission (no reflection) for normal incidence [8–10, 22]. Other than normal incidence, we expect the transmission probability to oscillate

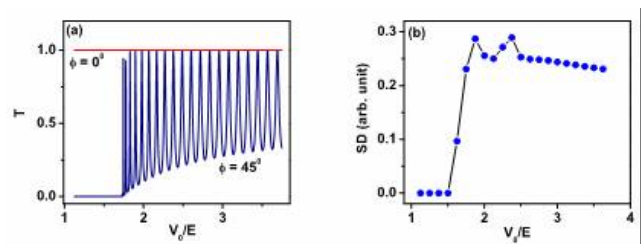


FIG. 5: (a) Transmission probability as a function of barrier height (with respect to the incident electron energy), calculated using the expression in the main text for incident angles  $\phi = 0^\circ$  (red) and  $\phi = 45^\circ$  (blue). For normal incidence ( $\phi = 0^\circ$ ), perfect transmission is observed for all values of the barrier height, while the transmission probability oscillates as a function of barrier height for  $\phi = 45^\circ$ . (b) Standard deviation of the transmission probability as a function of barrier height after balancing arms  $\phi = 0^\circ$  and  $\phi = 45^\circ$ .

as a function of angle of incidence. For a particular angle (other than normal incidence) the transmission probability will also oscillate as a function of barrier strength [10].

Our p-n\*-p (or n-p\*-n) devices include two p-n interfaces - one on either edge of the top gate. For a ballistic p-n junction, where the mean free path is larger than the p-n junction width, the transmission of Dirac electrons is perfect for normal incidence and is partially suppressed for other angles [8]. Under the application of bias, the first p-n junction preferentially transmits more carriers that are nearly normally incident to the barrier. These carriers arrive to the second p-n junction, which again selects more of the normally incident ones. As all the arms have the same width, and the branching point is less than  $l_{mfp}$  away from the top-gated portion, a large portion of the electrons coming from arm 1, that emerged in the direction normal to the pn junction, will go straight into arm 2. The current carried by the normally incident electrons along the arm 1-2 should be unaffected by the changing barrier height (controlled by  $V_{Tg}$ ). The arm 3 (or 4) is placed at an angle with respect to the top gate ( $\phi = 45^\circ$ ), so it will preferentially collect electrons that emerged at the angles close to  $\phi = 45^\circ$ . As the transmission probability oscillates as a function of the barrier height for any incident angles other than normal, the current flowing through angled arm 1-3 (or 1-4) is expected to oscillate as a function of  $V_{Tg}$ .

We note that it is not necessary for the entire device to be ballistic in order to observe the angle dependence of the resistance. As long as the difference in the current distribution due to ballistic effects in a small portion of the straight and angled arms is large enough, it will manifest as the deviation in the resistance from the balanced condition with changing top gate voltage. We also note that any gate-dependent angle insensitive series resistances will equally affect all arms and will not cause a deviation from the balanced condition. Since all the

arms share the same top-gated portion, there will be no differences in the pn-junction length and roughness, as well as other effects that might become important when comparing different physical devices.

Since the transmission probability does not depend on the barrier height (controlled by  $V_{Tg}$ ) for normal incidence, and it oscillates as a function of barrier height for other incident angles, we interpret the large fluctuation amplitude in  $R_{balance}$  in the p-n\*-p (or n-p\*-n) regime as due to the barrier height-dependent transmission probability of charge carriers at angles close to  $\phi = 45^\circ$ .

The transmission probability ( $T$ ) for an electron across a graphene p-n junction as a function of incident angle ( $\phi$ ) can be expressed in the following way [10];

$$T(\phi) = 1 - |r|^2, \text{ with}$$

$$r = 2ie^{i\phi} \sin(q_x d) \times$$

$$\frac{\sin \phi - ss' \sin \theta}{ss'[e^{-iq_x d} \cos(\phi + \theta) + e^{iq_x d} \cos(\phi - \theta)] - 2i \sin(q_x d)},$$

where  $k_F = 2\pi/\lambda$ ,  $k_x = k_F \cos \phi$ ,  $k_y = k_F \sin \phi$ ,  $q_x = \sqrt{(E - V_0)^2/(\hbar^2 v_F^2) - k_y^2}$ ,  $\theta = \tan^{-1}(k_y/q_x)$ ,  $s = \text{sgn}(E)$ ,  $s' = \text{sgn}(E - V_0)$ . We have taken the barrier width,  $d = 200$  nm.

For normally incident electrons ( $\phi = 0$ ), this equation gives  $T = 1$  and the transmission probability oscillates for any other incident angle. For a particular angle other than zero, the value of  $T$  oscillates with increasing energy of the potential barrier ( $V_0$ ). In Fig. 5(a) we show the variation of  $T$  as a function of  $V_0$  for  $\phi = 0$  and  $\phi = 45^\circ$ . It is evident that  $T = 1$  for  $\phi = 0$  and it is independent of the barrier height. However, for  $\phi = 45^\circ$  no transmission is observed for small values of the barrier height and  $T$  oscillates as function of  $V_0$ . For a device shown in Fig. 1(a) and the measurement schematic in Fig. 2(a), the deviation in the resistance from the balanced condition between arms 1-2 and 1-3 (or 1-4) is  $R_{balance} = R_{\phi=0^\circ} - R_{\phi=45^\circ}$ . Since each resistance is proportional to the transmission probability at the corresponding angle, we have  $R_{balance} \propto T(\phi = 45^\circ) - T(\phi = 0^\circ)$ . As the  $T(\phi = 0^\circ)$  is independent of  $V_0$ , the variation of  $R_{balance}$  as a function of  $V_0$  will be determined by the  $T(\phi = 45^\circ)$  alone. In order to compare the data to the theory, we calculated the standard deviation of  $T(\phi = 45^\circ)$  as a function of  $V_0$  by taking the average over bin size of 100 data points (step of  $V_0/E$  is 0.00125), shown in Fig. 5(b). It is clearly seen that the standard deviation remains zero initially, then it increases sharply and remains at a high value for  $V_0/E \gtrsim 2$ . This is qualitatively in good agreement with the experimental data shown in Fig. 4(a).

In Fig. 3(a)-(d) we found that from the balanced condition, the resistance does not show much variation as a

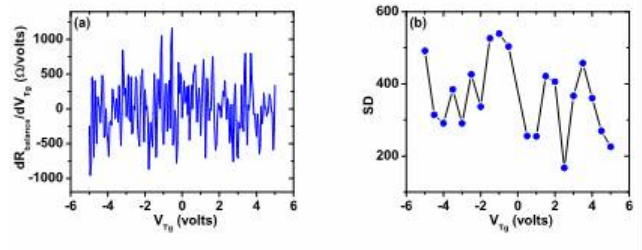


FIG. 6: (a)  $dR_{balance}/dV_{Tg}$  as a function of  $V_{Tg}$  measured by balancing arms 1-3 and 1-4 (see Fig. 2(a)), both of which are placed at a  $45^\circ$  angle with respect to the the top gate. The amplitude of the fluctuations remains nearly the same for all values of  $V_{Tg}$ . Corresponding standard deviation is shown in (b).

function of  $V_{Tg}$  in the p-p\*-p or n-n\*-n type device configuration. This rules out the possibility of any direction-insensitive cause of the fluctuations.

The conductance fluctuations in the p-p\*-p or n-n\*-n side as a function of  $V_{Tg}$  arise due to the quantum interference of backscattered quasiparticle wavefunctions, which changes due to the change in the chemical potential under the top gate with varying  $V_{Tg}$ . In the p-n\*-p or n-p\*-n side, the increase of the fluctuations from this "base line" is due to the contribution from the angle dependence of resistance. It is interesting to note that the amplitude of "base line" is larger in the p-p\*-p compared to the n-n\*-n side (see Fig. 3(c), (d) and Fig. 4(a) and(b)), its origin is not clear yet, but the percentage of the variation is the same in both cases (nearly four-fold increase in standard deviation is observed as a function of  $V_{Tg}$  in both Fig. 4(a) and (b)). Multiple reflections under the top-gated portion would contribute to the "base line" fluctuation, but would not result in a deviation from the balanced condition, as they would affect both arms equally.

To show that this excess fluctuation in the  $R_{balance}$  is entirely due to the contributions from the angle-dependent part of the resistance, we have also measured the variation of resistance by balancing the arms 1-3 and 1-4. We found that the variation in the  $R_{balance}$  remains nearly constant throughout the whole range of back gate and top gate voltage (see Fig. 6(a) and (b)). As both arms 3 and 4 are placed at  $45^\circ$  angle,  $V_{Tg}$  has nearly the same effect on the current distribution in these two arms, resulting in the same deviation of  $R_{balance}$  for any combination of back gate and top gate voltage. This clearly supports the claim that the increased fluctuations observed in Fig. 3(a)-(d) are due to the angle-selective transmission of charge carriers.

- 
- [1] Novoselov K. S., Geim A. K., Morozov S. V., Jiang D., Zhang Y., Dubonos S. V., Grigorieva I. V., & Firsov A. A. Electric field effect in atomically thin carbon films. *Science* **306**, 666-669 (2004).
- [2] Geim A. K., & Novoselov K. S., The rise of graphene. *Nat. Mater.* **6**, 183-191 (2007).
- [3] Castro Neto A. H., Guinea F., Peres N. M. R., Novoselov K. S. & Geim A. K. The electronic properties of graphene. *Rev. Mod. Phys.* **81**, 109-162 (2009).
- [4] Das Sarma S., Adam S., Hwang E. H. & Rossi E. Electronic transport in two-dimensional graphene. *Rev. Mod. Phys.* **83**, 407-470 (2011).
- [5] Ando T., Nakanishi T., & Saito R. Berry's Phase and Absence of Back Scattering in Carbon Nanotubes. *J Phys. Soc. Jpn.* **67**, 2857-2862 (1998).
- [6] Suzuura H., & Ando T. Crossover from Symplectic to Orthogonal Class in a Two-Dimensional Honeycomb Lattice. *Phys. Rev. Lett.* **89**, 266603 (2002).
- [7] Beenakker C. Andreev reflection and Klein tunneling in graphene. *Rev. Mod. Phys.* **80** 1337-1354 (2008).
- [8] Cheianov V. V., & Fal'ko V. I. Selective transmission of Dirac electrons and ballistic magnetoresistance of n-p junctions in graphene *Phys. Rev. B* **74** 041403 (2006).
- [9] Cheianov V. V., Fal'ko V. I., & Altshuler B. L. The Focusing of Electron Flow and a Veselago Lens in Graphene p-n Junctions. *Science* **315**, 1252-1255 (2007).
- [10] Katsnelson M. I., Novoselov K. S., & Geim A. K. Chiral tunnelling and the Klein paradox in graphene. *Nat. Phys.* **2**, 620-625 (2006).
- [11] Shytov A. V., Rudner M. S., & Levitov L. S. Klein Backscattering and Fabry-Perot Interference in Graphene Heterojunctions. *Phys. Rev. Lett.* **101**, 156804 (2008).
- [12] Park C.-H., Son Y.-W., Yang L., Cohen M. L., & Louie S. G. Electron Beam Supercollimation in Graphene Superlattices. *Nano. Lett.* **8**, 2920-2924 (2008).
- [13] Beenakker, C. W. J., Sepkhanov, R. A., Akhmerov, A. R. & Tworzydło, J. Quantum Goos-Hänchen effect in graphene. *Phys. Rev. Lett.* **102**, 146804 (2009).
- [14] Hartmann, R. R., Robinson, N. J. & Portnoi, M. E. Smooth electron waveguides in graphene. *Phys. Rev. B* **81**, 245431 (2010).
- [15] Low T. & Appenzeller J. Electronic transport properties of a tilted graphene p-n junction. *Phys. Rev. B* **80**, 155406 (2009).
- [16] Rossi E., Bardarson J. H. Brouwer P. W. & Das Sarma S. Signatures of Klein tunneling in disordered graphene p-n-p junctions. *Phys. Rev. B* 2010, **81**, 121408 (2010).
- [17] Sajjad R. & Ghosh A. High efficiency switching using graphene based electron optics. *Appl. Phys. Lett.* **99**, 123101 (2011).
- [18] Huard B., Sulpizio J. A., Stander N., Todd K., Yang B., & Goldhaber-Gordon D. Transport Measurements Across a Tunable Potential Barrier in Graphene. *Phys. Rev. Lett.* **98**, 236803 (2007).
- [19] Stander N., Huard B., & Goldhaber-Gordon D. Evidence for Klein Tunneling in Graphene p-n Junctions. *Phys. Rev. Lett.* **102**, 026807 (2009).
- [20] Young A. F., & Kim P. Quantum interference and Klein tunnelling in graphene heterojunctions. *Nat. Phys.* **5**, 222-226 (2009).
- [21] Wu Y., Perebeinos V., Lin Y.-M., Low T., Xia F., & Avouris P. Quantum Behavior of Graphene Transistors near the Scaling Limit. *Nano. Lett.* **12**, 1417-1423 (2012).
- [22] Gorbachev R. V., Mayorov A. S., Savchenko A. K., Horsell D. W., & Guinea F. Conductance of p-n-p Graphene Structures with Air-Bridge Top Gates. *Nano. Lett.* **8**, 1995-1999 (2008).
- [23] Williams J. R., Low T., Lundstrom M. S., & Marcus C. M. Gate-controlled guiding of electrons in graphene. *Nat. Nano.* **6**, 222-225 (2011).
- [24] Sonin E. B. Effect of Klein tunneling on conductance and shot noise in ballistic graphene. *Phys. Rev. B* **79**, 195438 (2009).
- [25] Fogler M. M., Novikov D. S., Glazman L. I., & Shklovskii B. I. Effect of disorder on a graphene p-n junction. *Phys. Rev. B* **77**, 075420 (2008).
- [26] Zhang L. M., & Fogler M. M. Nonlinear Screening and Ballistic Transport in a Graphene p-n Junction. *Phys. Rev. Lett.* **100**, 116804 (2008).
- [27] Sutar S., Comfort E. S., Liu J., Taniguchi T., Watanabe K., & Lee J. U. Angle-Dependent Carrier Transmission in Graphene pn Junctions. *Nano. Lett.* **12**, 4460-4464 (2012).
- [28] Xia F., Perebeinos V., Lin Y.-M., Wu Y., & Avouris P. The origins and limits of metal-graphene junction resistance. *Nat. Nano.* **6**, 179-184 (2011).
- [29] Giovannetti G., Khomyakov P. A., Brocks G., Karpan V. M., van den Brink J., & Kelly P. J. Doping Graphene with Metal Contacts. *Phys. Rev. Lett.* **101**, 026803 (2008).
- [30] Lee E. J. H., Balasubramanian K., Weitz R. T., Burghard M., & Klaus Kern K. Contact and edge effects in graphene devices. *Nat. Nano.* **3**, 486-490 (2008).
- [31] Huard B., Stander N., Sulpizio J. A., & Goldhaber-Gordon D., Evidence of the role of contacts on the observed electron-hole asymmetry in graphene. *Phys. Rev. B* **78**, 121402(R) (2008).